



Modelling the effect of geo-matrix conduction on the bulk and pore water resistivity in hydrogeological sedimentary beddings

N. J. George¹ · A. M. Ekanem¹ · J. E. Thomas¹ · T. A. Harry²

Received: 10 February 2021 / Accepted: 5 April 2021 / Published online: 18 April 2021
© The Author(s), under exclusive licence to Springer Nature Switzerland AG 2021

Abstract

Generally, the electrical method of geophysics is potentially valuable in typifying the subsurface conductivity and its surrounding medium. Sixteen datasets of 1-D electrical resistivity survey was integrated with 8 core samples, which were taken in the neighbourhood of eight of the sixteen VES datasets. The two sets of data were intertwined with geological and hydrogeological datasets to enhance the realization of unique results used in assessing the aquifer geo-matrix and pore water geo-resistivity in four counties in the coastal province of Akwa Ibom State, southern Nigeria. The current electrode separations of 1-D resistivity data were extended up to 300 m to ensure that the prolifically exploited water-bearing units were assessed. The VES data were manually and electronically modeled and each of them showed characteristic four geo-electric layers with KH, HK, KQ, HA and A group of curves. The core samples, which cut across the local Government Areas under survey, included sandy clay (12.5%), fine-grained sand (50.0%), medium-grained sand (12.5%) and coarse sand (25.0%). Bulk resistivities of water-bearing units and other primary geo-electrical indices were measured in all sixteen locations. However, in the eight aquifer core sample locations, water resistivities were measured in situ. The core samples were taken to the laboratory for measurements of fractional porosity and volumetric water content. The measured fractional porosity ranged from 0.189 to 0.267 with an average of 0.232, whilst volumetric water content varied from 0.23 to 0.31 with an average value of 0.268. The transmission coefficients were computed from volumetric water content and other parameters in the work. The values ranged from 0.4135 to 0.5612 with an average value of 0.4945. Fractional porosity was also modeled from field parameters and the results showed a good match with laboratory measurement as the root—mean square error was just 1.3%. Intrinsic specific resistance and conductivity of soil aquifer matrix were found to be $3.333 \times 10^3 \Omega\text{m}$ and $3.000 \times 10^{-4} \text{Sm}^{-1}$ respectively. The study has provided useful information about the geo-electrical and geo-pore properties of the prolifically exploited aquifers in the study area. The aquifer parameter contour maps have been delineated and these, together with other parameter relations generated in this study could help in predicting the volumetric conductivity between pore water and the matrix texture of hydrogeological units in the study area and other areas with similar geology.

Keywords Geo-matrix conductivity · Specific geo-resistance · Hydrogeological sediments · Volumetric water content · Transmission coefficient

✉ N. J. George
nyaknojjimmy@gmail.com; nyaknogeorge@aksu.edu.ng

A. M. Ekanem
anny4mart@yahoo.com

J. E. Thomas
jewelemem@gmail.com

T. A. Harry
tharry.tom@gmail.com; Thomasharry@aksu.edu.ng

¹ Department of Physics (Geophysics Research Group), Akwa Ibom State University, Ikot Akpaden, Nigeria

² Department of Geology, Akwa Ibom State University, Ikot Akpaden, Nigeria

Introduction

The magnitude of mobile electrical charges in the earth conducting unit or the valence of mobile electrical charges in soil is proportional to the water content as electrical charges in soils are mobile only in the hydrated form in the water-filled ducts or in water-thin layers/films around soil matrix (Rhoades et al. 1976). Temporal variability in the soil moisture profile can be estimated by using electrical resistivity geo-sounding data according to Aaltonen (2001) and Michot et al. (2003). The bulk or volume conductivity of a hydrogeological formation is the sum of the soil

matrix conductivity and water conductivity, which creates a medium for entanglements of the soil–water characteristics associated with Fractional porosity, temperature and salinity (Rhoades et al. 1977). The dissolved minerals in the soil water content have some time-invariant physical and chemical characteristics that influence soil water retention and the electrical properties of soil solution at varying considerably different water content conditions (Murad 2012). The solid phase characteristics relate to the texture and minerals infused in the volumetric water content. Therefore, the pore fluid composition is associated with electrical conductivity, which relates to the mobility of the ions present in the fluid filling the pores. The conductivity or resistivity depends on the concentration and the viscosity of the water (Scollar et al. 1990). The estimation of intrinsic matrix resistivity requires field measurements of volume/bulk resistivities and knowledge of the concentration of dissolved ions in the volumetric water contents, which is known to link with water resistivity (Cosoli et al. 2020). This paper aims at using geophysical technique, laboratory measurements and computational analyses in finding the pore-water resistivity dependent coefficients and the intrinsic matrix resistivity/conductivity, a constituent part of bulk resistivity measured in geo-resistivity/geo-conductivity studies.

The theoretical framework

The flow of current in the geo-pores obeys the condition of zero divergence of current density J , which is given in Eq. 1 as:

$$\nabla \cdot J = \nabla \cdot \left(\frac{I}{A} \right) = \nabla \cdot I = 0, \quad (1)$$

where A and I are area and electric current respectively. For electrical conductivity σ and a given electric potential ϕ , the current obeys Ohm's law such that it can be expressed as in Eq. 2:

$$I = -\sigma \nabla \phi. \quad (2)$$

In the soil medium, the current and the electrical conductivity are defined in terms of the bulk volume. If the electrical conductivity is assumed to be independent of the location, Laplace's equation can be obtained by combining Eqs. 1 and 2 as follows:

$$\nabla \cdot I = \nabla \cdot (-\sigma \nabla \phi) = 0. \quad (3)$$

The bulk soil conductivity or its inverse (resistivity) is a combination of two parallel conductors: the bulk liquid-phase conductivity, σ_1 , which is associated with the free salt in the liquid-filled pores and the bulk surface conductivity σ_s ,

associated with exchangeable ions at the solid/liquid surface. Their relation is given in Eq. 4:

$$\sigma_b = \sigma_1 + \sigma_s. \quad (4)$$

Generally, the volume/bulk electrical conductivity σ_b depends linearly on the conductivity of soil water σ_w . According to Seladji et al (2010), the fraction of the total cross-sectional area occupied by the liquid phase conducts current according to Eq. 5;

$$\sigma_b = \sigma_w \theta T + \sigma_s \quad (5)$$

where θ and T are the volumetric water content and the transmission coefficient respectively. The transmission coefficient gives information about the tortuous nature of the current lines and any observed reduction in the mobility of ion near the solid–liquid or liquid–gas boundaries. According to Michot et al. (2003), the relationship between volumetric water content and electrical resistivity for different sedimentary formation is given by

$$\frac{1}{\rho_b} = \frac{1}{\rho_w} (a\theta^2 + b\theta) + \frac{1}{\rho_m}, \quad (6)$$

where ρ_b , ρ_w and ρ_m are respectively bulk, water and solid matrix resistivities. The constants a and b are implicitly containing the soil and water characteristics, which include salinity, fractional porosity and temperature. These constants are assumed to be invariant with time. These parameters can be estimated by combining electrical resistivity survey and laboratory analysis of soil samples (Aaltonen 2001). Simplifying Eq. 6, we can obtain the relation between the constants and the transmission coefficient. Thus

$$\frac{1}{\rho_b} = \frac{1}{\rho_w} \theta (a\theta + b) + \frac{1}{\rho_m} = \frac{1}{\rho_w} \theta T + \frac{1}{\rho_m} = \sigma_w \theta T + \sigma_m, \quad (7)$$

where

$$T = a\theta + b. \quad (8)$$

Equation 8 is symmetric and analogous with Eq. 5 With measuring of θ and setting $\frac{1}{\rho_b} = \sigma_b$, T can be estimated using Eq. 9

$$T = \frac{\sigma_b - \sigma_m}{\theta \sigma_w}. \quad (9)$$

For various sedimentary formations and their water samples, σ_m can be determined as an intrinsic value from the intercept of $\frac{1}{\rho_b} - \frac{1}{\rho_w}$ plot in Eq. 7.

Study area and geology of the study area

The study area was found to lie between latitudes 4°45' to 4°35' N and longitudes 7°30' to 8°10' E and it is located in the southeastern sector of Nigeria. The location is contiguous with the hinterland of Atlantic Ocean lagoons as shown in Fig. 1. The survey area is on average, somewhat undulating with dominant Cuesta (crests with troughs and mild hills) caused by drainage. The terrain is geomorphologically known to have a smaller degree of ruggedness, low hills and lower relief (George 2020). The area has a closely spaced hydrographic network, which drains the area. The area has substantial quantity of rainfall with the mean annual rainfall fluctuating from 2 m and more than 3 m throughout the peak era. Yearly mean air temperature swings between 25 and 28 °C. The vegetation of the terrain ranges from tropical rainforest in the south, earth and west to derived grassland in the northern parts (George

et al. 2014). In the geological description, the coastal shorefront is obviously known for its three lithostratigraphical units of which the Akata Formation is the oldest (Eocene to recent) according to Akpan et al. (2013) and Peters et al. (1989). This geological Formation exists as pro-delta facies and functions as source rock (Short and Stauble 1967) for crude oil. It is thought that the shales of this formation were formed during the early development phases of Niger Delta Basin progradation and are intrinsically under-compacted and overpressured forming diapiric structures such as ridges and shale swells, which intrude into overlying younger Agbada Formation. Lying above the Akata Formation is the Agbada Formation, which is dominant throughout Niger Delta clastic wedge. This formation houses the main reservoir and seal for crude oil accumulation in the basin and is known to be mainly parallel delta front facies with the largest thickness of about 4 km or 13,000 feet (Sort and Stauble 1967). These lithologies comprise the irregular sequences of sands,

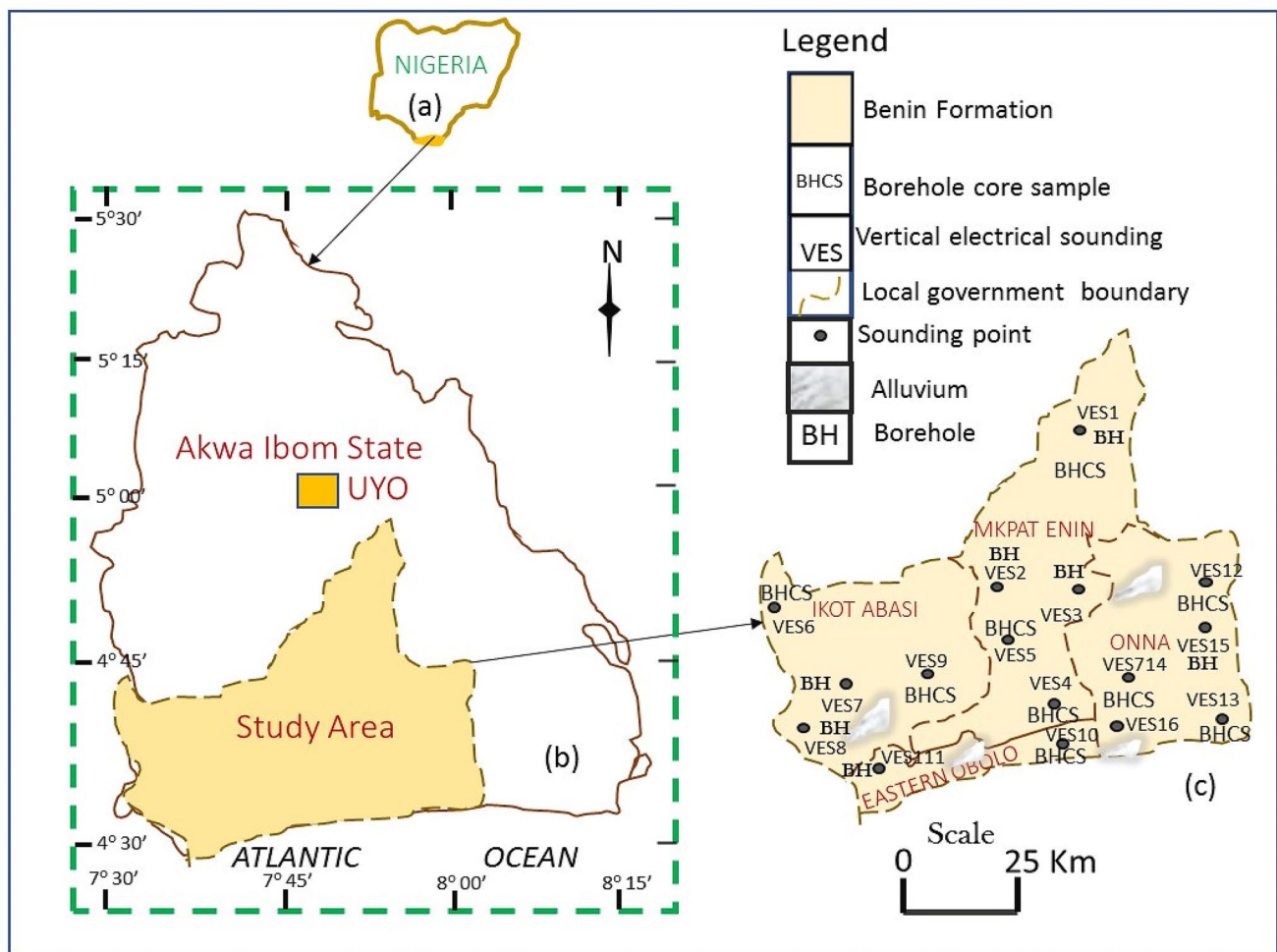


Fig. 1 Schematic map of **a** Nigeria showing, the location of **b** Akwa Ibome, which indicates the study area and **c** the study area showing the local geology, VES points, borehole cored sample points, borehole locations and the local government boundaries

silts and shales that are arranged within 3–30 m successions, which are defined by progressive upward changes in bed thickness and grain size. The depositional environment of the Agbada Formation is mostly interpreted to be fluvial–deltaic environment. The base of the formation outspreads beyond 4.5 km or 4600 feet in some areas and is well-defined by the youngest marine shale, while the shallow parts of the formation are composed of non-marine sand deposited in alluvial or upper coastal plain environments during progradation of the delta (Doust and Omatsola 1989). The youngest Benin Formation in which the study is centered comprises the top part of the basin clastic wedge, from the Benin–Onitsha area in the north to beyond the coast line (Short and Stauble 1967). The macrostructures in Niger Delta Basin swings from simple rollover faults, multiple growth faults, antithetic faults and collapsed crest faults (Evamy et al 1978; Stacher 1995; Reijers 2011; Onuoha and Dim 2017). These sediments are formed during the Late Eocene to Early Oligocene with the reservoirs mainly controlled by pre- and syn-sedimentary tectonic elements responsible for mutable rates of subsidence and sediment supply (Doust and Omatsola 1989; Reijers 2011). The aquifer samples considered were generally brownish and thought to be formed from moderately coarse-textured alluvium George (2015a). Intrinsically, the soils have grayish brown, and marginally finer texture sometimes interposed with gravels.

Materials and methods

The possibility of assessing the effect of geo-matrix conduction effect on the bulk and pore water geo-resistivity in hydrogeological sedimentary units (aquifers and its overlying and underlying layers) was through the use of core samples, water samples, resistivity metre and its accessories for measurement of bulk/volumetric earth resistances, which were inverted to specific resistances or resistivities, and conductivity metre for measurement of water conductivity/resistivity. These materials, together with laboratory tools were paramount in arriving at the results stated this work. The methods used include: the field geophysical measurements, laboratory analysis and computational/numerical analysis of the data acquired. The hybrid of these integrated method provided the necessary information that actualized the realization of the aim of this research.

Field measurements of bulk resistivities, water resistivity and laboratory determination of volumetric water content from core samples

In this survey, sixteen (16) vertical electrical soundings (VES) spread within the mapped area were performed, using

resistivity metre (ABEM SAS 1000). The chosen configuration was Schlumberger, which was used to quantify the volume/bulk earth's resistivity vertically and horizontally within the maximum electrode separations. Direct currents were artificially injected into the earth. The injected current generated electric fields that were equivalent to the electric potentials in the subsurface (George et al. 2011). The generated potential paved the way for measurements of apparent bulk resistivities, thickness and depth, regarded as primary indices in geo-resistivity measurements (Ekanem et al. 2019; George et al 2020). Resistivity measurements were performed following a classical four-electrode configuration: an electrical current (I) was injected by two electrodes referred to as A and B and the resulting electrical potential difference (ΔV) was measured by two other electrodes, M and N. The four electrodes are collectively known as a quadrupole. The ratio $\left(\frac{\Delta V}{I}\right)$, an apparent electrical resistance (ΔV), was measured and converted into apparent resistivity (ρ_a) by the resistivity meter. This conversion depends on the geometrical features of the quadrupole (the orientation and relative distances between the four electrodes). For the chosen configuration, the separations of current electrodes (AB) were expressively greater than the separation of potential electrodes (MN) (Akpan et al. 2013). In the half current electrode separation (AB/2), 150 m was and while 2 m was minimum. In (MN/2), 60 m and 0.5 m respectively maximum and minimum. The ρ_a of the subsurface was gauged from the measured R_a using appropriate geometric factor given in Eq. 10.

$$\rho_a = \pi \left(\frac{\left(\frac{AB}{2}\right)^2 - \left(\frac{MN}{2}\right)^2}{MN} \right) \left(\frac{\Delta V}{I} \right) = G \times R_a, \quad (10)$$

where $G = \pi \left(\frac{\left(\frac{AB}{2}\right)^2 - \left(\frac{MN}{2}\right)^2}{MN} \right)$. The outliers, non-geologic

equivalent in the measurements were smoothed by manual plot of ρ_a against $\frac{AB}{2}$. The true bulk resistivity ρ_b , thickness and depth of the subsurface geologic layers were estimated by the inversion of the apparent resistivity data using a Win Resist software program. The interpretation was constrained by borehole data. The bulk resistivities for all the formation within the maximum current separations were taken in all the sixteen locations earmarked for the study. Eight out of the sixteen locations had core samples for the formations adjudged as aquifers. The eight (8) boreholes with water and core samples were specifically earmarked for measurements of in situ water electrical conductivity using electrical conductivity (EC) and volumetric water content θ . Conductivity metre terminals were inserted into water and by pressing the conductivity button; the liquid crystal display recorded the

conductivity of water. This was done severally to take the mean value, for quality assurance. Based on the inverse relation between resistivity and conductivity, resistivity equivalent value of conductivity for each borehole was obtained as ρ_w . The core samples of water-bearing units obtained during drilling at the indicated depth of boreholes were shipped to the laboratory for measurements of volumetric water content (θ). Volumetric water content was determined by finding the percentage of water content by weight in the aquifer sample and multiplying the aquifer water content by its bulk density (Rowell 1994; Friedman 2005). To determine gravimetric water content (θ_g) of aquifer, the saturated aquifer sample from the field was weighed and the oven dried at 105 °C periodically until there was no more loss in weight, which indicated that all of the water has been dried from the sample. Coding the wet mass of aquifer as M_w and the dry mass of aquifer as M_d , the θ_g was determined as mass difference between the wet and dry samples of aquifer per unit mass of dry sample of aquifer or as the mass of water in aquifer sample per mass of dry aquifer and is given as represented in Eq. 11:

$$\theta_g = \frac{M_w - M_d}{M_d} \tag{11}$$

The above equation alludes to the fact θ_g is the mass of water in the aquifer per unit mass of solid particles (soil matrix) and each gram of soil matrix in hydrogeological unit contains a specific gram of water. With the measurement of gravimetric water content θ_g , volumetric water content θ was estimated using the bulk density of aquifer sample (β_a) and water density (β_w) in (g/cm³) through the expression given by.

$$\theta = \theta_g \times \frac{\beta_a}{\beta_w} = \theta_g \times \beta_a \tag{12}$$

where β_w is 1 g/cm³. Porosities were also determined from core samples using the procedure of mean wet weight (W_w)—dry weight (W_d) analysis according to Emerson (1968), Gelehouse (1971) and George et al. (2015a). For the volume of core sample (V) soaked for eighteen hours in distilled water boiled for thirty minutes (30 min) in a vacuum pressure at 0.3 mBar and taking the cleansing procedures of opined by API (1960) and Emerson (1968), the effective fractional porosities for the eight-core samples were estimated using Eq. 13:

$$\phi_{Lab} = \frac{W_w - W_d}{V} \tag{13}$$

According to Archie (1942), the average pore geometry factor ($a_f = 0.5245$) and cementation factor ($m_f = 1.5431$) estimated in the area, by George et al (2015a), were used to gauge the fractional porosities (ϕ_E) taking into

consideration, the formation factor ($F = \frac{\rho_b}{\rho_w}$) as required in the expression in Eq. 14

$$\rho_b = \rho_w \times \frac{a}{\phi^m} \Rightarrow \phi_E = \left(\frac{a_f}{F}\right)^{\frac{1}{m_f}} \tag{14}$$

According to Waxman and Smits (1968), the bulk interface conductivity σ_s , between water and the surface matrix can be predicted through Eq. 15.

$$\sigma_s = \frac{B \cdot Q_v}{F} \tag{15}$$

where B is the equivalent conductance of clay exchange cations in Sm² meq⁻¹ and Q_v is the cation exchange capacity per unit pore volume in meq m⁻³. Using Eq. 15 average σ_s for the eight boreholes was estimated using the plot of their $\frac{1}{F}$ against their corresponding water resistivity ρ_w according to the linearized Waxman-Smits’s model (George et al. 2015a) in Eq. 16.

$$\frac{1}{F} = \frac{1}{Fi} + \left(\frac{QB_v}{Fi}\right) \cdot \rho_w \tag{16}$$

The term Fi is the characteristic formation factor, which connotes the formation factor for medium that is free of clay. Using intercept—slope terms in the regression of Eq. 16, the average σ_s was estimated using Eq. 15.

Results and discussion

The results of electrical resistivity characteristics performed at the location of the borehole agreed with the geologic profiles from top to bottom and showed a succession of deviations in geology within and between the geologic columns penetrated by currents. Figure 2 illustrates some samples of the VES data correlated with boreholes near their locations. The construed VES shows good correlations with the borehole and this guarantees quality assurance in this applied method (Hodlur et al. 2006; George et al. 2011; George 2020). The specific resistance values show that the current that penetrated the subsurface passed through sequences of arenites, argillites and intercalations of fine and coarsening formation textures as the rise and fall in the values of bulk resistivity at different depths in Fig. 2 and Table 1 indicate. This is in tandem with the conclusions of investigators who characterized the mapped area (Fig. 1) Benin Formations inundated with arenites intercalated with minor argillites (Petters 1989; Obianwu et al. 2011; Ibuot et al. 2013; George et al. 2014; Ibanga and George 2016; Ibanga and George 2016; Ekanem et al. 2019; George 2020). Table 1 shows the summary of the resistivity, depth penetrated by current, thickness and curve

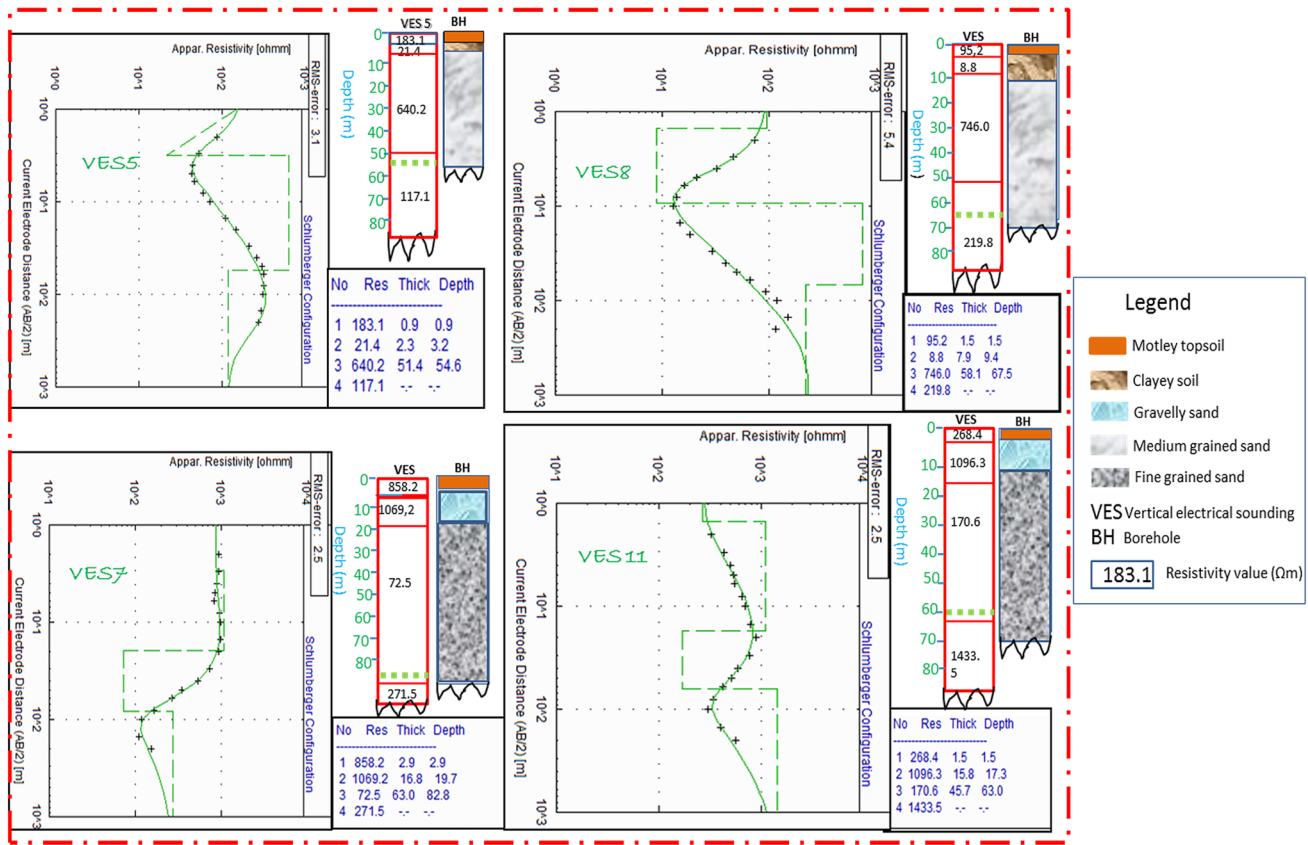


Fig. 2 Correlation of VES curves and the nearby lithology formation in the study area

type acquired through the use of vertical electrical sounding technique otherwise known as electrical drilling technique. Current penetrated four layers except VES 16 that showed that current penetrated three layers. The formations penetrated by currents are discernible from the low and high resistivities described mostly by H and K curve types. As established on Table 1 KH ($\rho_1 < \rho_2 > \rho_3 < \rho_4$) curve type was found in VES 2, 3, 4, 6, 7, 9, 11, 14, and 15. Other curve types were HA ($\rho_1 > \rho_2 < \rho_3 < \rho_4$) in VES 10, 12 and 13; HK ($\rho_1 > \rho_2 < \rho_3 > \rho_4$) in VES 5 and 8; KQ ($\rho_1 < \rho_2 > \rho_3 > \rho_4$) in VES 1 and A ($\rho_1 < \rho_2 < \rho_3$) in VES 16. As a matter of fact, the chart in Fig. 3 shows that by percentage of curve distribution, KH has 56.3%, followed by HA, HK, KQ and A curve types, which respectively have 18.7%, 12.5% and 12.5%. The curve distributions show considerably the high and low bulk resistivity values in the study area (George et al. 2016a, b). The different geologic units exhibit uncorrelated ranges of bulk resistivity probably due to the dissolved leachates of fauna, flora and minerals from geochemical sources during groundwater flow within the subsurface. In the inferred layer one, the resistivity ranges from 95.2 to 3455.5 Ωm with a mean of 855.3 Ωm . Layer two showed a bulk resistivity range of 8.8 to 3606.6 Ωm with

a mean value of 1235.5 Ωm . Similarly, layers three and four displayed ranges and averages of 72.5–1464.5 Ωm and 117.1–8367.3 Ωm and 698.6 Ωm and 2005.6 Ωm respectively. The uncorrelated inversion of bulk resistivity with depths, a deviation from what is theoretically believed, is a clear indication of the intercalation of arenites and argillites as well as dissolution of minerals in the geogenic formation (Ibanga and George 2014). The area exhibits varying thicknesses and depths for the geologic formation therein. The thickness of layer one ranges from 0.5 to 19.6 m with mean 3.5 m. Layer is characterized with thickness range and mean of 1.6–56.7 m and 17.3 m, respectively. The thickness in layer three, except VES 16 fully assessed by the maximum current electrode separations ranges from 16.1 to 89.2 m with mean 51.1 m. The maximally exploited hydrogeological units in the study area cut across this range of thickness at their indicated depth. The depths of geologic units that characterize the easily exploitable aquifers have these ranges and averages from top to bottom within the maximum current electrode separation used. Layer one ranged from 0.5 to 19.6 m with mean 8.2 m. In layer two and three the depth ranges and averages are 2.1 to 76.3 m and 20.5 to 113.1 m and 24.7 m and 72.3 m respectively. The saturated depths from the

Table 1 Summary of geophysics survey in the study area

VES	Location	Coordinate degree		No of layer	Layer resistivity (Ohm-m)				Layer thickness (m)			Layer depth (m)			Curve type	
		Lat	long		ρ_1	ρ_2	ρ_3	ρ_4	Δx_1	Δx_2	Δx_3	D_1	D_2	D_3		
1	Mkpat Enin	4.7752	7.7854	4	666.5	3606.6	1054.6	375.7	5.3	24.9	32.4	5.3	30.2	62.6	KQ	
2	Mkpat Enin	4.7345	7.7733	4	401.6	1108.4	481.9	1195.9	1.1	27.5	50.5	1.1	28.6	79.1	KH	
3	Mkpat Enin	4.7034	7.8758	4	395.7	1567.1	510.3	1808.6	0.6	7.9	49.3	0.6	8.5	57.8	KH	
4	Mkpat Enin	4.6067	7.8167	4	660.4	1488.6	549.2	1248.7	1.3	3.6	47.8	1.3	4.9	52.7	KH	
5	Mkpat Enin	4.6535	7.7332	4	183.1	21.4	640.2	117.1	0.9	2.3	51.4	0.9	3.2	54.6	HK	
6	Ikot Abasi	4.6984	7.5511	4	949.9	2715.5	1464.5	3745.2	0.5	3.9	16.1	0.5	4.4	20.5	KH	
7	Ikot Abasi	4.6117	7.6317	4	858.2	1069.2	72.5	271.5	2.9	16.8	63.0	2.9	19.7	82.8	KH	
8	Ikot Abasi	4.5767	7.5684	4	95.2	8.8	746.0	219.8	1.5	7.9	58.1	1.5	9.4	67.5	HK	
9	Ikot Abasi	4.6184	7.7086	4	718.4	1844.9	1362.2	1440.8	0.5	1.6	80.8	0.5	2.1	82.9	KH	
10	Eastern Obolo	4.5184	7.8757	4	1433.0	210.0	860.5	8367.3	19.4	43.1	49.6	19.4	62.5	112.1	HA	
11	Eastern Obolo	4.5453	7.6359	4	268.4	1096.3	170.6	1433.5	1.5	15.8	45.7	1.5	17.3	63.0	KH	
12	Onna	4.7172	8.0167	4	1721.4	118.2	611.2	4893.0	19.6	56.7	36.8	91.6	76.3	113.1	HA	
13	Onna	4.5689	8.0278	4	3455.5	1825.6	393.9	2030.4	0.6	2.0	89.2	0.6	2.6	91.8	HA	
14	Onna	4.5997	7.8832	4	1157.0	1318.3	735.6	1585.9	1.1	37.0	47.8	1.1	38.1	85.9	KH	
15	Onna	4.6629	8.0098	4	156.4	800.8	407.8	1350.1	1.3	9.1	47.9	1.3	10.4	58.3	KH	
16	Onna	4.5871	7.8753	3	563.4	966.1	1115.9	-	1.1	75.1	-	1.1	76.2	-	A	
Range					95.2–3455.5	8.8–3606.6	72.5–1464.5	117.1–8367.3	0.5–19.6	1.6–56.7	16.1–89.2	0.5–91.6	2.1–76.3	20.5–113.1		
Mean					855.3	1235.3	698.6	2005.6	3.7	17.3	51.1	8.2	24.7	72.3		

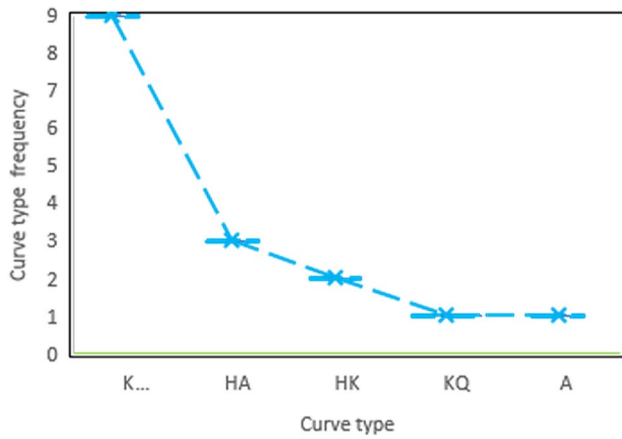


Fig. 3 Curve type frequency distribution in the study area

borehole information and information from inferred geoelectric primary indices indicate that the geologic columns within and below water table are characterized by stratigraphic sequences of sands ranging from fine to coarse sands (George et al. 2016b; Ekanem et al. 2019).

In attempt to investigate the effects of the interactions between the water in the formation pores and geomatrix, which determine the bulk conductivity σ_b , or the bulk resistivity ρ_b , eight (8) available core samples from aquifer spread in four counties investigated at their indicated depths and geo-electric characteristics in Table 2, were taken undisturbed to the laboratory for estimation of volumetric water content using the procedure explained in the method using Eq. 12. The dry textures of the referred hydrogeological units of the eight-core samples are given in Fig. 4. The samples ranged from fine sand (549.2–860.5 Ωm) to coarse sands (1362.2–1464.5 Ωm) with one sandy clay (393.9 Ωm). The value in brackets (Fig. 4) represents ρ_w estimated for each of the aquifer geologic units while the higher values in Ohm-m represent the ρ_b .

According to Eqs. 13 and 14, the core sample effective laboratory porosities ranging from 0.189 to 0.267 with mean 0.232 and the porosities calculated by juxtaposing petrophysical parameters with water resistivities ranging from 0.190 to 0.250 with mean 0.221 were determined and presented in Table 2. The determined values of effective porosities of the hydrogeological units from the two techniques are highly correlated and this shows the goodness of fit of the average cementation factor and pore geometry factor determined for similar geologic units in some parts of the study area by George et al. (2015a). The Root-Mean Square (RMS) value for the estimated values of porosities from the laboratory-measured value and the parameter estimated values using the expression in Eq. 17 is 1.3%. This indicates an excellent tie between the two estimators.

Table 2 Summary of results from geophysics measurements, laboratory analysis of core samples and computation from combined results

S/N	ρ_b (Ohm-m)	ρ_w (Ohm-m)	ϕ_E	ϕ_{Lab}	σ_b (S/m)	σ_w (S/m)	θ	T	D_g (m)	D_d (m)	Geologic texture
1	549.2	100.79	0.219	0.229	0.001821	0.009921	0.28	0.5286	52.7	51.9	Fine sand
2	1464.5	250.10	0.209	0.221	0.000683	0.003998	0.25	0.4559	20.5	24.9	Coarse sand
3	1362.2	250.90	0.220	0.240	0.000734	0.003986	0.25	0.4538	82.9	80.9	Medium grained sand
4	860.5	140.20	0.203	0.219	0.001162	0.007133	0.26	0.4649	112.1	109.8	Fine sand
5	393.9	59.10	0.192	0.189	0.002539	0.016915	0.23	0.4135	91.8	89.9	Sandy clay
6	611.2	130.20	0.241	0.251	0.001636	0.007680	0.31	0.5612	113.1	100.4	Fine sand
7	640.2	143.90	0.250	0.267	0.001562	0.006949	0.30	0.5611	54.6	51.6	Fine sand
8	1115.9	225.40	0.233	0.237	0.000896	0.004437	0.27	0.5168	76.2	77.0	Medium grained sand
Range	393.9–1464.5	59.1–250.9	0.19–0.25	0.189–0.267	0.000683–0.002539	0.003986–0.016915	0.23–0.31	0.4135–0.5612			
Mean	874.7	162.6	0.221	0.232	0.001379	0.007627	0.268	0.4945			

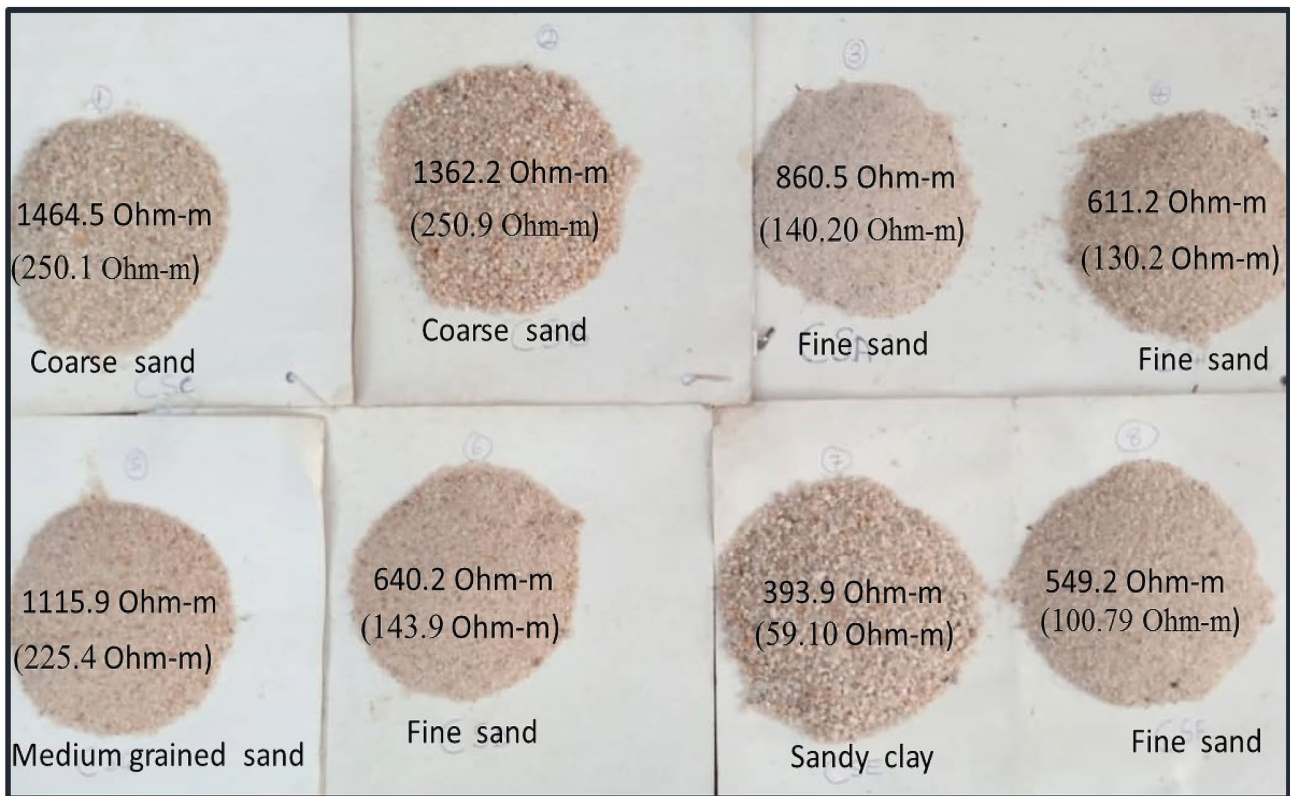


Fig. 4 Dried samples of cored hydrogeological units showing their textures, measured bulk resistivity (ρ_b) in Ohm-m and their corresponding water resistivity (ρ_w) in brackets

$$RMS = \sqrt{\frac{1}{n} \sum_{i=1}^n (\phi_{Obs}^i - \phi_{Model}^i)^2}, \tag{17}$$

where n is number of data points, ϕ_{Obs}^i is the observed porosity from each of the core samples, ϕ_{Model}^i is the modelled porosity at a given data point obtained from formation parameters and $i = 1, 2, 3, \dots$

The values of ϕ_{Lab} and θ_E determined from Eqs. 13 and 14 respectively were plotted against the volumetric water content determined from Eq. 12. The graph in Fig. 5 suggests direct and linear relations of porosities (ϕ_{Lab} and θ_E) with the volumetric water content as each, respectively, has high coefficient of determination 0.9943 and 0.9828 and Eqs. 18 and 19.

$$\phi_{Lab} = 1.1409\theta - 0.0204 \tag{18}$$

$$\phi_E = 1.213\theta + 0.0007 \tag{19}$$

Equations 18 and 19 can be used to determine porosity when the volumetric water content is available and vice versa. The gradients (m) in the graphs represent the

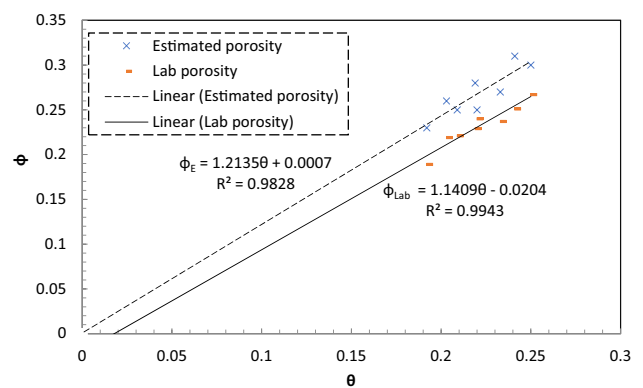


Fig. 5 Showing the plots of estimated and laboratory-measured porosities against volumetric water content for eight assessed core samples of aquifer units

effective porosity—volumetric water content ratio, which account for the degree of water saturation in the aquifer. For unsaturated aquifer, $m < 1$ and $m > 1$ for saturated aquifer characterized by well-connected pores. The reality of the value of m , which is greater than 1 (i.e. 1.14 and 1.21 for ϕ_{Lab} and ϕ_E respectively) is that the assessed hydrogeological units characterized by volumetric

water content range of 0.23–0.31 have pores with high connectivity.

The soil and water conduction properties for the eight assessed core samples were investigated using a plot of $\frac{1}{\rho_b}$ against $\frac{1}{\rho_w}$ in Fig. 6. The graph showed a high coefficient of determination (0.9194) and hence, a high degree of correlation between bulk conductivity and water conductivity (see Eq. 20).

$$\frac{1}{\rho_b} = 0.1415 \frac{1}{\rho_w} + 0.0003 \tag{20}$$

Typically, the regression line has a slope of 0.1415 representing $(a\theta^2 + b\theta)$ and intercept of 3×10^{-4} S/m or 3333 Ω m representing average conductivity/resistivity of aquifer matrix (i.e. $\frac{1}{\rho_m}$ or σ_m) in Eq. 6. With the estimated value of matrix resistivity, the resulting resistivity in the aquifer is usually influenced when it is saturated with water and hence the variation in the values of measured resistivities and conductivities. The simplification of Eq. 6 in Eq. 7 led to the formation of Eq. 8, the transmission coefficient (T), which gives information about the tortuous nature of the current flow between solid–liquid boundaries. Plotting T against the volumetric water content according to Eq. 8 gave a graph in Fig. 7. The graph revealed with a high coefficient of determination (0.9543), a slope and an intercept of $(a = 1.9913)$ and $(b = -0.0407)$, respectively, when comparing Eq. 8 with Eq. 21 below:

$$T = 1.9913\theta - 0.0407 \tag{21}$$

The intrinsic constants a and b , which are implicitly containing the soil and water characteristics such as salinity, fractional porosity and temperature are assumed to be naturally invariant with time (Aaltonen 2001). Based on this revelation and according to Rhoades et al. (1976), the average threshold

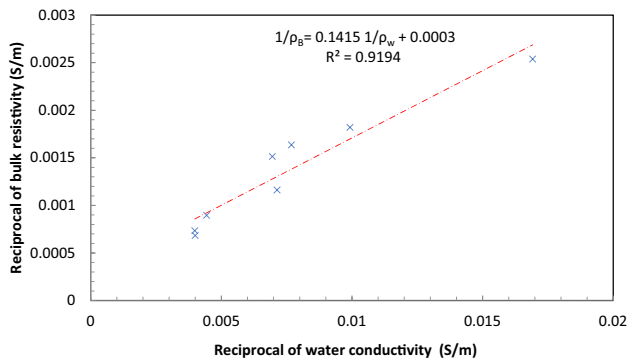


Fig.6 A graph of $\frac{1}{\rho_b}$ against $\frac{1}{\rho_w}$ within the eight assessed core samples of aquifer units

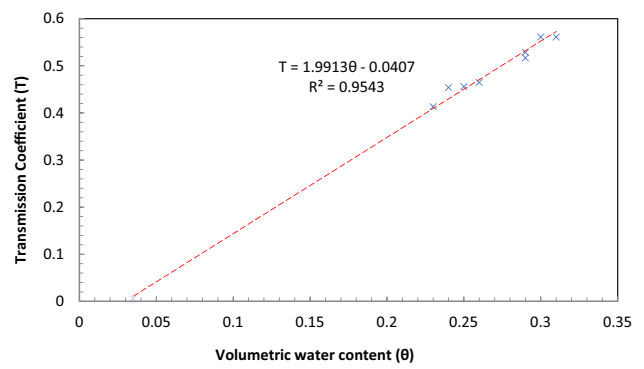


Fig.7 A graph of transmission coefficient against volumetric water content in the eight assessed core samples of aquifer units in the study area

volumetric water content given as $-\left(\frac{b}{a}\right)$ is 0.0204. This computational derivation agrees with the intercept on the θ –axis of Fig. 7, the average threshold volumetric water content for the study area. Solving for θ in the quadratic term equivalent to the slope of the plot of $\frac{1}{\rho_b}$ against $\frac{1}{\rho_w}$, i.e. $(a\theta^2 + b\theta)$, in conjunction with the determined average values of the constants a and b , in Eq. 20, the bounds of volumetric content of ions dissolved in water stand at 0.0914–0.1415. This constituent part of the volumetric water content accounts for the dissolved ions contributed by water and aquifer units responsible for mobile electrical charges in the earth conducting unit in the study area. The bulk interface conductivity σ_s , between water and the surface matrix, theorized by Waxman and Smits (1968) in Eq. 15 ($\sigma_s = \frac{BQ_v}{F}$) can be predicted through the intercept-slope relationship of the regression analysis of Eq. 16 (George et al. 2015a). The $\frac{1}{F} - \rho_w$ plot roughly gives an intercept ($\frac{1}{F_i} = 0.176$) and slope ($\frac{BQ_v}{F_i} = 6 \times 10^{-5} Sm^{-1}$) in Eq. 22:

$$\frac{1}{F} = 6 \times 10^{-5} \rho_w + 0.176 \tag{22}$$

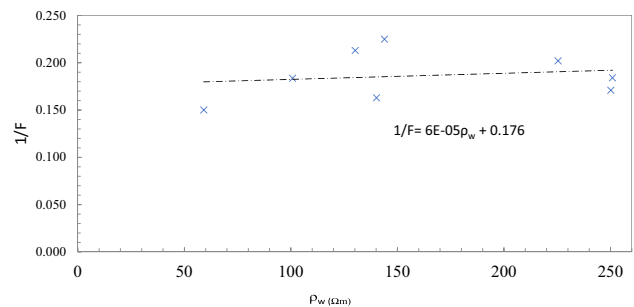


Fig.8 $\frac{1}{F} - \rho_w$ plot in the eight assessed aquifer core samples

The poorly correlated nature of points in the graph of Fig. 8 is an indication of the differential textures of the aquifer core samples used. From the deduced parameters, the intrinsic formation factor is 5.682 and product of B (the equivalent conductance of clay exchange cations in $\text{Sm}^2\text{meq}^{-1}$) and Q_v (the cation exchange capacity per unit pore volume in meqm^{-3}) gave an average bulk interface conductivity of $6 \times 10^{-5} \text{Sm}^{-1} \times 5.682$ ($3.4092 \times 10^{-4} \text{Sm}^{-1}$). Consequently, the surface conductivities of the eight assessed aquifer unit core samples, with average $3.35 \times 10^{-5} \text{Sm}^{-1}$ was found to be ranging from $5.1151 \times 10^5 \text{Sm}^{-1}$ at Onna near, VES 13 to $7.66298 \times 10^{-5} \text{Sm}^{-1}$ in Mkpato Enin, near VES 5. This exploit was achieved from the slope of the $\frac{1}{\rho_b} - \rho_w$ plot, with reference to Eq. 15. The conductivity of the hydrogeological units is partly accounted for by the presence of clay in the aquifer samples and partly due to dissolution of conducting ions in the hydrogeological units (Palacky 1987; Hunt et al. 1995). The representative core samples (50% of the total sample points) used in assessing the bulk and pore water conduction effect on the hydrogeological sedimentary beddings of the study area are well representing the other 50% VES points that core samples were not available. This is because the range of bulk resistivity and the depth of investigations in the entire study area are almost within the 50% core sample representative areas. This assertion can be assessed through the two-dimensional modeled images of the aquifer bulk resistivity and aquifer depth of investigation of the study area in Figs. 9 and 10, respectively. The bulk resistivity distribution identifies that one of the aquifer samples with the lowest resistivity dominates mainly parts of Ikot Abasi and Eastern Obolo. The fine sand occupies a large

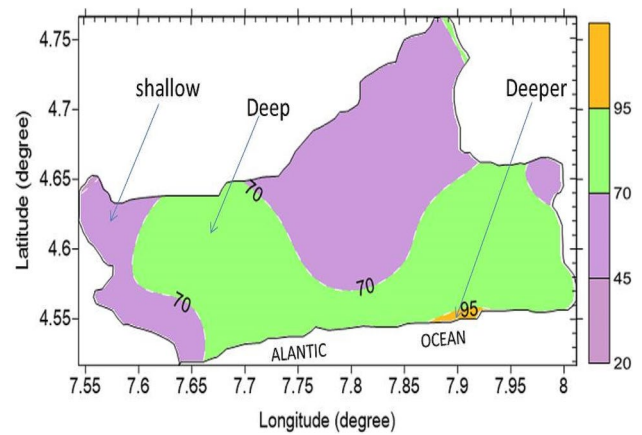
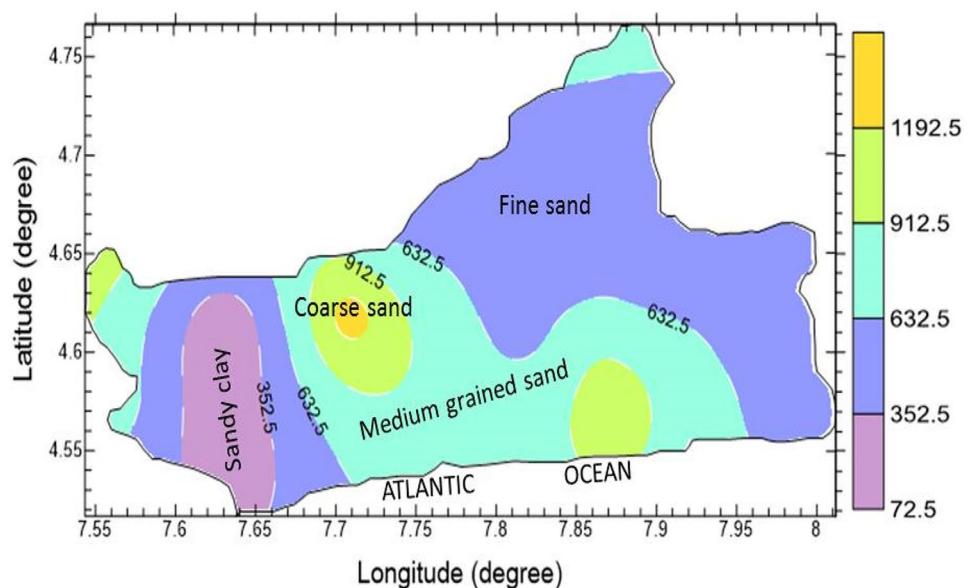


Fig.10 Aquifer depth (m) of investigation distribution in the entire study area

portion of Mkpato Enin and Onna whilst parts of Ikot Abasi and Eastern Obolo show a smaller chunk of fine aquifer units. The medium-grained and coarse sand hydrogeological units are sparsely distributed in Onna and Ikot Abasi and they extend into the Atlantic Ocean. As indicated on the contour map of Fig. 9, the hydrogeological units are naturally distributed at their indicated depths. The geophysics results comfortably agree with the geology as the assessed aquifer unit core samples range from sandy clay—to coarse sands also inferred from geophysics. In Fig. 10, depths greater than 70 m were found in all the local government counties investigated around the Atlantic Ocean. Glaringly, Fig. 10 indicates that depths between 20 and 70 m are predominantly seen in Mkpato Enin thinly found in Ikot Abasi and Onna. Again, the distributions of aquifer depths are also

Fig. 9 Aquifer bulk resistivity (Ωm) distribution in the entire study area



controlled by natural geologic processes such as weathering, erosion/attrition of geologic sediments, transportation, depositions and phenomenal lithification of sediments (George et al. 2019). The geophysics results can be generalized within the mapped area as depths (D_g) of inferred aquifer units from geophysics are in sync with the depths (D_d) of the eight-core samples obtained directly during drilling in Table 2. The aquifer water resistivity as indicated on the contour map of Fig. 11 shows a gradual decrease in water resistivity from east to west with very minimal inversion in parts of Mkpát Enin and Onna counties. The noticeable distribution can be attributed to the distribution of geologic units and ease of ingress of salinity into the groundwater depositories (George et al. 2020). Hydrogeological units that are susceptible to interaction with water from saline sources are reasoned to have lower water resistivity and higher conductivity (George et al. 2015b; Ekanem et al. 2019). Hence, aside from the dissolution of leachates from organic sources and minerals from inorganic sources, ingresses of salinity, which may come from the Atlantic Ocean into the vulnerably permeable hydrogeological units, are more likely foreseeable in the eastern parts of the study area than the western parts as the low water resistivity scenario in the geologic units in these areas suggests.

The mass of water distributed per unit mass of soil depends on the bulk density, which determines the volumetric water content from the gravimetric water content. In the study area, the volumetric water content for the eight-core samples (50% of the total sample points) that were available is contoured in Fig. 12 to show its distribution in the study area. The distribution from Fig. 12 indicates that the study area has more argillites (formations known to be characterized by high volumetric water content), (Rhoades et al. 1976; Seladji et al. 2010) than arenites (loose sandy formations with lower volumetric water content) in the northern parts than the southern parts. This is coherent with higher values of volumetric water content in the north (mostly north of

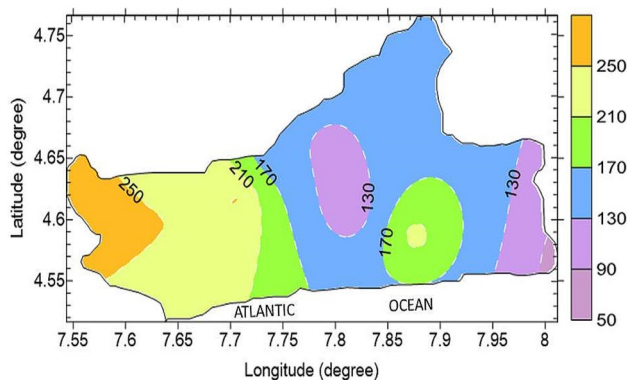


Fig. 11 Aquifer water resistivity (Ωm) distributions within the geologic core samples

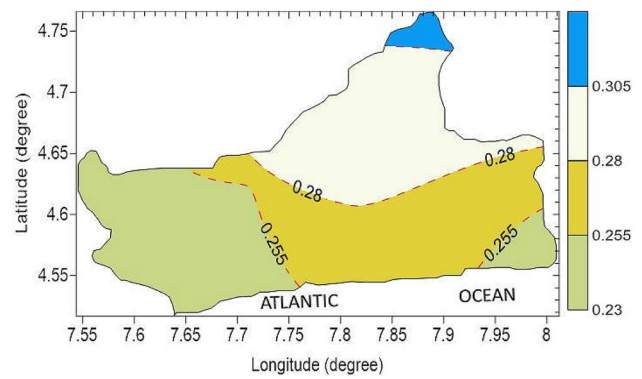


Fig. 12 Volumetric water content of aquifer unit core samples

Mkpát Enin) than the southern parts, spreading across all the four counties under survey. This inferred characteristic of the hydrogeological units in the study area also affects the porosity in the same trend. This is because they are directly related. This revelation is symptomatic of the inter-gain/inter-matrix composition, which finally gives the physical and the electrical properties of the hydrogeological units in the study area. Consequently, the northern parts of the study area have hydrogeological units that are denser whilst the southern parts that are contiguous to the Atlantic Ocean are looser. As earlier demonstrated through graph of Fig. 7, the transmission coefficient is dependent on the volumetric water content. The distribution in Fig. 13 replicates the distribution of volumetric water content. Therefore, the coefficient of water transmission is comparatively higher in the northern parts of Mkpát Enin whilst the entire southern parts of the study area are characterized by lower values (Fig. 13). This suggests that the tortuous path of current lines between the matrix-water boundaries of the aquifer unit in the study area is higher with higher volumetric water content as its distribution on the contour map reveals.

Generally, using the field, laboratory and computational techniques discussed so far, the summary of the determined

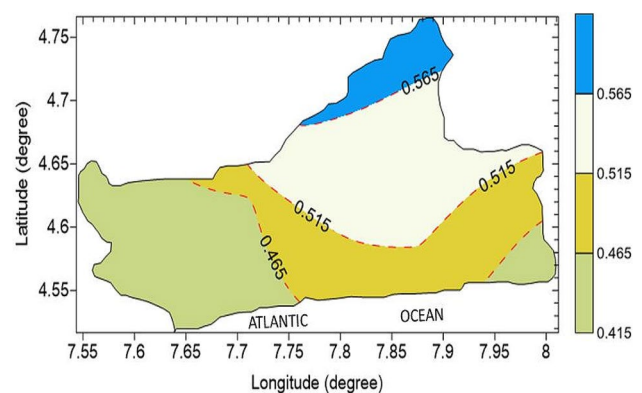


Fig. 13 Transmission coefficient of aquifer unit core samples

Table 3 Fundamental representative properties of hydrogeological units

Property	Value
Intrinsic specific resistance/resistivity of soil aquifer matrix	$3.333 \times 10^3 \Omega\text{m}$
Intrinsic conductivity of soil aquifer matrix	$3. \times 10^{-4} \text{Sm}^{-1}$
Average of <i>a</i> constant	1.9913
Average of <i>b</i> constant	−0.0407
Average threshold volumetric water content	0.0204
Bounds of volumetric content of ions dissolved in water	0.0914 – 0.1415
Bulk average interface conductivity (BQ_v)	$3.4092 \times 10^{-4} \text{Sm}^{-1}$
Average surface conductivity (σ_s)	$3.35 \times 10^{-5} \text{Sm}^{-1}$
Average formation factor	5.682
Average volumetric water content	0.268
Average transmission coefficient	0.4945
Average fractional porosity	0.232
Average depth of exploited aquifer	72.3 m
Average thickness of exploited aquifer	51.1 m
Cementation factor (m_f) by George et al (2015a)	0.5245
Pore geometric factor (a_f) by George et al (2015a)	1.5431

fundamental representative properties of hydrogeological units are presented on Table 3 are considered to be useful in shoring up the criteria for exploration and exploitation of hydrogeological units in the coastal shorefront of south-western Nigeria.

Conclusion

Assessment of geo-matrix conduction effect on the bulk and pore water geo-resistivity in hydrogeological sedimentary beddings was undertaken to unravel the effects of geo-matrix on the bulk pore water resistivity through the combination of field, laboratory and computational analyses. The results show that the amount of mobile electrical charges in aquifer unit is sensitive to the volumetric water content of geologic units and transmission coefficient that soar up in water-filled ducts or in water-thin layers/films around soil matrix. The study applied 1-D VES datasets whose interpretations were controlled by boreholes near them, as well as core and water sample analyses to ascertain that the average bulk matrix conductivity/resistivity as $3.0 \times 10^{-4} \text{Sm}^{-1}/3.333 \times 10^3 \Omega\text{m}$ in the mapped area. The laboratory determination of fractional porosity agreed favourably well with fractional porosity determined from field geophysics models with a root mean square error of 1.3%. The study area, which is characterized by low and high resistivities as curve types indicate, has elevated volumetric water contents and transmission coefficients in areas away from the shore of Atlantic Ocean. This natural distribution concludes that water depositories are looser than areas away from the Atlantic Ocean. The study area identifies the average interface conductivity of $3.4072 \times 10^{-4} \text{Sm}^{-1}$, which alludes to the presence of

small pockets of clay in the hydrogeological units. Relations governing the dynamic properties of aquifer units have been established and they can be excellent tools in predicting the volumetric properties of aquifer units. The spatial distributions of primary geo-electrical indices and volumetric properties through 2-D contour maps have been delineated in this work for clearer and thoughtful explanations of conductivity with aquifer matrix-water ensemble. The summary of average dynamic properties of prolifically exploitable aquifer units delineated for the study area in Table 3 is indispensable for the integration of spatial variability of geologic units through field and laboratory analyses.

Acknowledgements The authors are indebted to Akwa Ibom State University for providing the wherewithal used in acquiring the field data and interpretation of data that led to the achievement of results presented in this manuscript.

Funding The project was funded by the authors through their research allowance from Akwa Ibom State University.

Declarations

Conflict of interest The author declares that he has no conflict of interest.

Human and animal rights This article does not contain studies with human or animal subjects.

References

- Aaltonen J (2001) Seasonal resistivity variations in some different swedish soils. *Eur J Environ Eng Geophys* 6:33–45

- Akpan AE, Ugbaja AN, George NJ (2013) Integrated geophysical, geochemical and hydrogeological investigation of shallow groundwater resources in parts of the Ikom-Mamfe Embayment and the adjoining areas in Cross River State, Nigeria. *Environ Earth Sci* 70(3):1435–1456. <https://doi.org/10.1007/s12665-0132232-3>
- American Petroleum Institute, API (1960) Recommended practice for core analysis. Rep No 40:55
- Archie GE (1942) The electrical resistivity log as an aid in determining some reservoir characteristics. *Am Inst Mineral Metal Eng Petrol Technol* 8–13 (**Technical publication 1422**)
- Cosoli G, Mobili A, Tittarelli F, Revel GM, Chiariotti P (2020) Electrical resistivity and electrical impedance measurement in mortar and concrete elements: a systematic review. *Appl. Sci* 10(24):9152. <https://doi.org/10.3390/app10249152>
- Doust H, Omatsola E (1989) Niger Delta. In: Edwards JD, Santogrossi PA (eds) Divergent/passive margin basins, vol 48. American Association of Petroleum Geologists Memoir, Tulsa, pp 201–238
- Ekanem AM, George NJ, Thomas JE, Nathaniel EU (2019) Empirical relations between aquifer Geohydraulic—geolectric properties derived from surficial resistivity measurements in parts of Akwa Ibom State, southern Nigeria. *Nat Resour Res.* <https://doi.org/10.1007/s11053-019-09606-1>
- Emerson AE (1968) A revision of the fossil genus Ulmeriella (Isoptera, Hodotermitidae, Hodotermitinae). *Am Museum Novit* 2332:1–22
- Evamy BD, Haremboure J, Kamerling P, Knaap WA, Molloy FA, Rowlands PH (1978) Hydrocarbon habitat of tertiary Niger Delta. *Am Assoc Pet Geol Bull* 62:277–298
- Friedman SP (2005) Soil properties influencing apparent electrical conductivity: a review. *Comput Electron Agric* 46:45–70
- Galehouse JS (1971) Sedimentation analysis. In: Carver RF (ed) Procedures in sedimentary petrology. Wiley-Interscience, New York, p 653
- George NJ (2020) Appraisal of hydraulic flow units and factors of the dynamics and contamination of hydrogeological units in the littoral zones: a case study of Akwa Ibom State University and its Environs Mkpato Enin L.G.A., Nigeria. *Nat Resour Res.* <https://doi.org/10.1007/s11053-020-09673-9>
- George NJ, Obianwu VI, Obot IB (2011) Estimation of groundwater reserve in unconfined frequently exploited depth of aquifer using a combined surficial geo-physical and laboratory techniques in the Niger Delta, South—South, Nigeria. *Adv Appl Sci Res* 2:163–177 (**Pelagia Research Library (USA) AASRFC**)
- George NJ, Ekong UN, Etuk SE (2014) Assessment of economically accessible groundwater reserve and its protective capacity in Eastern Obolo Local Government Area of Akwa Ibom State, Nigeria, using electrical resistivity method. *Int J Geophys* 2014:1–10. <https://doi.org/10.1155/2014/578981> (**Hindawi Publishing Company**)
- George NJ, Ibuot JC, Obiora DN (2015a) Geoelectrohydraulic parameters of shallow sandy aquifer in Itu, Akwa Ibom State (Nigeria) using geo-electric and hydrogeological measurements. *J Afr Earth Sci* 110:52–63. <https://doi.org/10.1016/j.jafrearsci.2015.06.006>
- George NJ, Emah JB, Ekong UN (2015b) Geohydrodynamic properties of hydrogeological units in parts of Niger Delta, southern Nigeria. *J Afr Earth Sci* 105:55–63
- George NJ, Akpan AE, Ekanem AM (2016a) Assessment of textural variation pattern and electrical conduction of economic and accessible quaternary hydroclastic facies via geoelectric and laboratory methods in SE Nigeria: a case study of select locations in Akwa Ibom State. *J Geol Soc India* 88(4):517–528
- George NJ, Akpan AE, Evans UF (2016b) Prediction of geohydraulic pore pressure gradient differentials for hydrodynamic assessment of hydrogeological units using geophysical and laboratory techniques: a case study of the coastal sector of Akwa Ibom State Southern Nigeria. *Arab J Geosci* 9(4):1–13
- George CF, David IMM, Spagnolo M (2019) Deltaic sedimentary environments in the Niger Delta, Nigeria. *J Afr Earth Sci* 160:103592. <https://doi.org/10.1016/j.jafrearsci.2019.103592>
- George NJ, Bassey NE, Ekanem AM, Thomas JE (2020) Effects of anisotropic changes on the conductivity of sedimentary aquifers, southeastern Niger Delta, Nigeria. *Acta Geophys* 68:1833–1843. <https://doi.org/10.1007/s11600-020-00502-4>
- Hodlur GK, Dhakate R, Andrade R (2006) Correlation of vertical electrical sounding and borehole-log data for delineation of saltwater and freshwater aquifers. *Geophysics* 71(1):G11–G20. <https://doi.org/10.1190/1.2169847>
- Hunt CP, Moskowitz BM, Banerjee SK (1995) Rock physics and phase relations—a handbook of physical constants. *Magn Prop Rocks Min Am Geophys Union AGU Ref Shelf* 3:189–204
- Ibanga JJ, George NJ (2016) Estimating geohydraulic parameters, protective strength, and corrosivity of hydrogeological units: a case study of ALSCON, Ikot Abasi, southern Nigeria. *Arab J Geosci* 9(5):1–16. <https://doi.org/10.1007/s12517-016-2390-1>
- Ibuot JC, Akpabio GT, George NJ (2013) A survey of the repository of groundwater potential and distribution using geo-electrical resistivity method in Itu Local Government Area (L.G.A.), Akwa Ibom State, southern Nigeria. *Cent Eur J Geosci* 5(4):538–547. <https://doi.org/10.2478/s13533-012-0152-5>
- Michot D, Benderitter Y, Dorigny A, Nicoulaud B, King D, Tabbagh A (2003) Spatial and temporal monitoring of soil water content with an irrigated corn crop cover using electrical resistivity tomography. *Water Resour Res* 39:1138
- Obianwu VI, George NJ, Udofia KM (2011) Estimation of aquifer hydraulic conductivity and effective porosity distributions using laboratory measurements on core samples in the Niger Delta, southern Nigeria. *Int Rev Phys Praise Worthy Prize Italy* 5(1):19–24
- Omar Faruk Murad (2012) Obtaining chemical properties through soil electrical resistivity. *J Civ Eng Res* 2(6):120–128. <https://doi.org/10.5923/j.jce.20120206.08>
- Onuoha KM, Dim CIP (2017) Developing unconventional petroleum resources in Nigeria: an assessment of shale gas and shale oil prospects and challenges in the inland Anambra Basin. In: Onuoha KM (ed) Advances in petroleum geoscience research in Nigeria, Chapter 16, 1st edn. University of Nigeria, Nsukka, pp 313–328
- Palacky GV (1987) Resistivity characteristics of geologic targets, in *Electromagnetic Methods in Applied Geophysics*, vol 1, Theory, 1351
- Petters SW (1989) Akwa Ibom State: physical background, soil and land use and ecological problems. Technical Report for Government of Akwa Ibom State, p 603
- Reijers TJA (2011) Stratigraphy and sedimentology of the Niger Delta. *Geologos* 17(3):133–162
- Rhoades JD, Raats PAC, Prather RJ (1976) Effect of liquid phase electrical conductivity, water content, and surface conductivity on bulk soil electrical conductivity. *Soil Sci Soc Am J* 40:651–655
- Rhoades JD, Kaddah MT, Halvorson AD, Prather RJ (1977) Establishing soil electrical conductivity salinity calibration using four electrodes cells containing undisturbed soil cores. *Soil Sci* 123:137–141
- Rowell DL (1994) Soil science: methods and applications. United Kingdom: Lonman Group
- Scollar I, Tabbagh A, Hesse A, Herzog I (1990) Archaeological prospecting and remote sensing. p 674
- Seladji S, Cosenza P, Tabbagh A, Ranger J, Richard G (2010) The effect of compaction on soil electrical resistivity: a laboratory investigation. *Eur J Soil Sci* 61(6):1045–1055. <https://doi.org/10.1111/j.1365-2389.2010.01309>
- Short KC, Stauble AJ (1967) Outline of the geology of Niger Delta. *Assoc Petrol Geol Bull* 54:761–779
- Stacher P (1995) Present understanding of the Niger Delta hydrocarbon habitat. In: Oti MN, Postma G (eds) *Geology of deltas*. A.A. Balkema, Rotterdam, pp 257–267

Uwa UE, Akpabio GT, George NJ (2019) Geohydrodynamic parameters and their implications on the coastal conservation: a case study of abak local government area (LGA) Akwa Ibom State, Southern Nigeria. *Nat Resour Res* 28:349–367. <https://doi.org/10.1007/s11053-018-9391-6>

Waxman MH, Smits LJM (1968) Electrical conductivities in oil-bearing shaly sand. *Soc Petrol Eng J* 8:107–122

Publisher's Note Springer Nature remains neutral with regard to jurisdictional claims in published maps and institutional affiliations.